



Available online at [www.sciencedirect.com](http://www.sciencedirect.com)

**ScienceDirect**

*Advances in Space Research* 63 (2019) 1318–1335

**ADVANCES IN  
SPACE  
RESEARCH**  
(*a COSPAR publication*)  
[www.elsevier.com/locate/asr](http://www.elsevier.com/locate/asr)

# GRACE accelerometer calibration by high precision non-gravitational force modeling

Florian Wöske\*, Takahiro Kato, Benny Rievers, Meike List

*University of Bremen, Center of Applied Space Technology and Microgravity (ZARM), 28359 Bremen, Germany*

Received 15 June 2018; received in revised form 15 October 2018; accepted 17 October 2018

Available online 25 October 2018

---

## Abstract

The precise modeling and knowledge of non-gravitational forces acting on satellites is of big interest to many scientific tasks and missions. Since 2002, the twin GRACE satellites have measured these forces in a low Earth orbit with highly precise accelerometers, for about 15 years. Besides the significance for the GRACE mission, these measurement data allow the evaluation of modeling approaches and the improvement of force models. Unfortunately, before any scientific usage, the accelerometer measurements need to be calibrated, namely scale factor and bias have to be regularly estimated.

In this study we demonstrate an accelerometer calibration approach, solely based on high precision non-gravitational force modeling without any use of empirically or stochastically estimated parameters, using our in-house developed satellite simulation tool XHPS. The aim of this work is twofold, first we use the accelerometer data and the residuals resulting from the calibration to quantitatively analyze and validate different non-gravitational force model approaches. In a second step, we compare the calibration results to three different calibration methods from different authors, based on gravity field recovery, GPS-based precise orbit determination, and based on modeled accelerations.

We consider atmospheric drag forces and winds, as well as radiation forces due to solar radiation pressure, albedo, Earth infrared and thermal radiation (TRP) of the satellite itself. For TRP, we investigate different transient temperature calculation approaches for the satellite surfaces with absorbed power from the aforementioned radiation sources. A detailed finite element model of the satellite is utilized for every force, considering orientation, material properties and shadowing conditions for each element.

For cross-track and radial direction, which are mainly affected by the radiative forces, our calibration residuals are quite small when drag is not super dominant ( $1\text{--}3 \text{ nm/s}^2$  for total accelerations around  $\pm 50 \text{ nm/s}^2$ ). For these directions the calibration seems to perform better than the other compared methods, where some bigger differences were found. For the drag dominated along-track direction it is vice versa, here our method is not sensitive enough because the difference between modeled and measured drag is bigger (e.g. residuals around  $10 \text{ nm/s}^2$  for total accelerations around  $\pm 70 \text{ nm/s}^2$  for low solar activity). In along-track direction the orbit determination based methods are more sensitive and produce more reliable results. Results for the complete GRACE mission time span from 2003 to 2017 are shown, covering different seasonal environmental conditions.

© 2018 COSPAR. Published by Elsevier Ltd. All rights reserved.

**Keywords:** Accelerometer calibration; Non-gravitational force modeling; GRACE

---

## 1. Introduction

The demand for highly accurate non-gravitational force modeling is increasing steadily. The growing quality of

measurement methods and sensors imposes the need to accurately consider and model all physical effects acting on satellites. This includes not only gravitational forces, but also all other forces, credited to non-gravitational sources. These forces originate from radiation of Sun, Earth and the satellite itself, as well as residual atmosphere. Detailed force models are a prerequisite for accurate orbit

---

\* Corresponding author.

E-mail address: [florian.woeske@zarm.uni-bremen.de](mailto:florian.woeske@zarm.uni-bremen.de) (F. Wöske).

propagation as well as for orbit determination from all kinds of measurement data, utilizing precise orbit determination (POD) techniques (e.g. Wu et al., 1991; Jäggi et al., 2006). Therefore the knowledge of non-gravitational forces, and thus sophisticated modeling capabilities, is of high importance for a variety of tasks related to accurate measurements from satellites. Examples are GNSS, satellite altimetry, or satellite geodesy, where accurate position of a satellite is required. Nevertheless, it is a common strategy to apply and estimate numerical and stochastic parameters to compensate for modeling deficiencies. With the development of precise models for non-gravitational forces, we try to reduce these stochastic parameters and thus enhance scientific results eg. for satellite gravimetry.

For satellite geodesy, the knowledge of the non-gravitational forces has an additional significance. In satellite geodesy, the gravitational field of a body is derived from the motion of satellites in this field. To determine solely the gravitational effects, the non-gravitational forces acting on the satellites have to be known.

A prominent geodesy mission is the Gravity Recovery And Climate Experiment (GRACE) which is designed to recover the gravitational field of the Earth and its time-dependent variations with unrivaled precision (Tapley et al., 2004). Two nearly identical satellites are following each other along-track in a polar orbit and continuously measuring the relative distance between each other. Additionally, they are equipped with GPS receivers, star cameras and high precision accelerometers to measure the non-gravitational forces acting on the satellites. The combination of measurements from these components enables the determination of the gravitational field of the Earth very accurately. The satellites were launched in 2002 and provided data for about 15 years. Meanwhile, the successor mission GRACE-Follow-On was successfully launched on 22nd of May 2018 to continue this work with just a short gap between both missions.

The main measurement for gravity field recovery (GFR) from GRACE data is the inter-satellite range which is determined with an accuracy of a few tenth of a  $\mu\text{m}$ . Because the knowledge of the non-gravitational accelerations is fundamental for GFR, they are measured with the accelerometers. In order to use the GRACE accelerometer data, they need to be continuously calibrated (Bettadpur, 2009; Van Helleputte et al., 2009). Previous studies have shown, that the calibration parameters are highly sensitive to temperature changes and are subject to non constant drift (Klinger and Mayer-Gürr, 2016).

Accelerometer calibration is performed in different ways. During the GFR process, the calibration parameters can be estimated along with the gravity field and other parameters (e.g. Klinger and Mayer-Gürr, 2016). Another approach is using reduced-dynamic POD based on GPS observations, utilizing accelerometer measurements as non-gravitational accelerations and estimating the calibration parameters. It has been shown that this approach needs strong constraints, especially for the bias in cross-

track and radial direction, and works best with a good a priori bias estimation (Van Helleputte and Visser, 2008; Van Helleputte et al., 2009). Also the GFR approach produces better gravity field solutions with a priori estimated bias values (Klinger and Mayer-Gürr, 2016). A different approach is the determination of the total acceleration by differentiation of the kinematic positions or velocities, and subtracting modeled gravitational forces. Because positions and velocities are in general derived from a GPS based POD, this method is also POD based. The general problem to overcome with this approach is the amplification of noise during differentiation, as well as accurate gravity modeling. This was shown by Bezděk (2010) and refined and analyzed in a broader way by Calabia et al. (2015).

In this study we present a calibration method solely based on precisely modeled non-gravitational accelerations. First we use the accelerometer data to validate our non-gravitational force models. Because the accelerometer measurements need to be calibrated, a direct evaluation of the models with the data is not possible, although they should measure the same quantity. Therefore we calibrate the accelerometer measurements with modeled accelerations for different modeling approaches and compare the resulting residuals. By residuals the remaining difference between calibrated accelerometer data and modeled accelerations is meant. Additionally some acceleration time series comparisons are shown. Subsequently, the calibration results are compared to results from different authors and methods. For that purpose, results were generously provided by: (Calabia et al., 2015) - a GPS based calibration, (Mayer-Gürr et al., 2016) - co-estimated calibration parameters within the GFR process, and (Klinger and Mayer-Gürr, 2016) - a force model based method. The last mentioned method is used as an intermediate step in the GFR process of Mayer-Gürr et al. (2016), to provide an a priori accelerometer calibration. In this study it is used as independent calibration method for comparisons. Additionally the calibration from the GRACE technical note TN-02 (Bettadpur, 2009), which is intended to be used as a preliminary approximation, is used for comparison.

The non-gravitational force models, applied in this study, are based on a detailed finite element (FE) model of the satellite. We consider atmospheric forces and winds, as well as radiation forces due to solar radiation pressure (SRP), albedo (ALB), Earth infrared (IR) and thermal radiation pressure (TRP) of the satellite itself. The TRP calculation from Rievers et al. (2016) and Rievers and Lämmerzahl (2011) is extended for transient and conductive satellite surface temperature calculation and arbitrary radiation sources (e.g. from ALB and IR). The ALB and IR force models are based on one hourly data from Clouds and the Earth's Radiant Energy System (CERES) (Wielicki et al., 1996). For each force the FE model is utilized, considering the orientation of each element with respect to the disturbance source, material properties as well as shadowing conditions with respect to satellite attitude (List et al., 2015).

All models are implemented in the generic satellite simulation tool XHPS (*eXtended High Performance satellite dynamics Simulator*) (Wöske et al., 2016), which is developed at ZARM in cooperation with the German Aerospace Center (DLR) in the collaborative research center geo-Q.

## 2. GRACE data

The two GRACE satellites, denoted as GRACE-A and -B, were launched in a nearly polar orbit with an altitude of about 500 km and an inclination of about 89°. The altitude slowly decayed over the years to about 350 km in 2017 (cf. Fig. 12 in Section 6.2).

Nearly all science sensor data of the two satellites are publicly available at processing level 1B (L1B) (Case et al., 2010). All satellite related sensor measurements are given in the satellite fixed science reference frame (SRF), shown in Fig. 1. The origin of that frame is located in center of mass (CoM) of the satellite, the x-axis is perpendicular to the satellites front panel, the z-axis is perpendicular to the bottom panel and the y-axis is concluding the right-hand system (Bettadpur, 2012).

In science mode, the satellites are pointing at each other with their x-axis (line of sight direction) and maintain this pointing with an accuracy of less than 0.5° for all three axes. The actual attitude is measured by two star cameras. The distance of about 200 km between both satellites results in a nominal flight path angle of about ±1° depending on which satellite is the leading and which is the trailing one. Because the orbits of both satellites are not exactly the same, also a small sideslip angle is present, but never exceeds 1°. Therefore drag is mainly acting in  $x_{SRF}$  direction. The  $y_{SRF}$  axis is nearly perpendicular to the orbital plane, hence the z-axis is closely nadir pointing. X-, y- and z-axis are also often referred as along-track, cross-track and radial direction, respectively, which originally correspond to the orbital frame (x towards orbital velocity, z normal to orbit plane). Leading and trailing satellite were switched two times in end of 2005 and mid 2014.

Because of the nearly constant attitude, with respect to the orbital frame, the pattern of the non-gravitational accelerations acting on the satellites is mainly determined by the orientation of the orbit with respect to the Sun. A

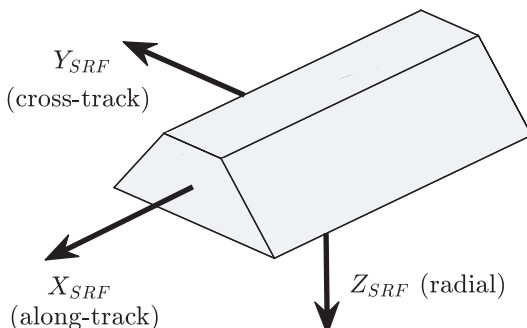


Fig. 1. Sketch of a GRACE satellite with the body fixed science reference frame (SRF), with its origin at the CoM of the satellite.

measure for this is the  $\beta'$  angle, which is defined as the smaller angle between the orbital plane and the vector pointing from Earth towards Sun. The precession of the polar GRACE orbit causes a change of the  $\beta'$  angle with a period of 322 days and between about ±85° (cf. Figs. 10 and 11 in Section 6.2) (Herman et al., 2012).

### 2.1. Accelerometer data (ACC1B)

The GRACE satellites are equipped with identical superSTAR accelerometers manufactured by ONERA (Touboul et al., 1999). These are three-axes electrostatic servo-controlled accelerometers, capable of measuring the three linear accelerations, as well as the three rotational accelerations. The sensor consists of a test mass, which is kept motionless with respect to its housing. The control forces to maintain the constant distance between housing and test mass is proportional to the non-gravitational forces acting on the sensor/satellite. The test mass CoM and the satellite CoM need to coincide, otherwise rotational motions introduces additional accelerations and coupling. The resolution of the linear accelerations is about  $10^{-10} \text{ ms}^{-2}/\sqrt{\text{Hz}}$  for the two sensitive axis (along-track and radial) and  $10^{-9} \text{ ms}^{-2}/\sqrt{\text{Hz}}$  for the less sensitive axis (cross track) for frequencies above 30 mHz. (Touboul et al., 2004; Flury et al., 2008).

The accelerometer is very sensitive to temperature variations, which is why it is operated in a thermally controlled environment. Nevertheless, small temperature changes occur and influence the accelerometer measurements. Because of battery restrictions, in the later years of the mission, thermal control was reduced since April 2011. A correlation of the  $\beta'$  angle, the accelerometer temperature and estimated calibration parameters is clearly visible and discussed more deeply in Section 6.2 and e.g. Klinger and Mayer-Gürr (2016). Recommendations for bias and scale are given in the GRACE technical note TN-02 (Bettadpur, 2009). They are estimated from GPS based POD and GFR results with data from launch until 2009. These bias estimates are given in the form of a quadratic function of time, and are intended to be used as a preliminary approximation. Note, that the advertised data should be used with following calibration equation:  $ACC_{corr} = \mathbf{s}(ACC1B + \mathbf{b})$  (Calabia, 2018; Calabia et al., 2015; Bettadpur, 2018), which is different than that given in TN-02 (For comparison see Eq. (1) in Section 3 for the conventionally used form of the calibration equation).

Additionally to sensor related errors, the accelerometer also measures disturbances introduced by the satellite itself. The most dominant effect are the activations of the cold-gas attitude control thrusters, which couple in all axes of the accelerometer and are clearly visible in the L1B accelerometer data. These firings happen about 600 times a day. Also heater switches and magnetic torquer effects couple in the data but with much less intensity (Peterseim et al., 2012; Flury et al., 2008).



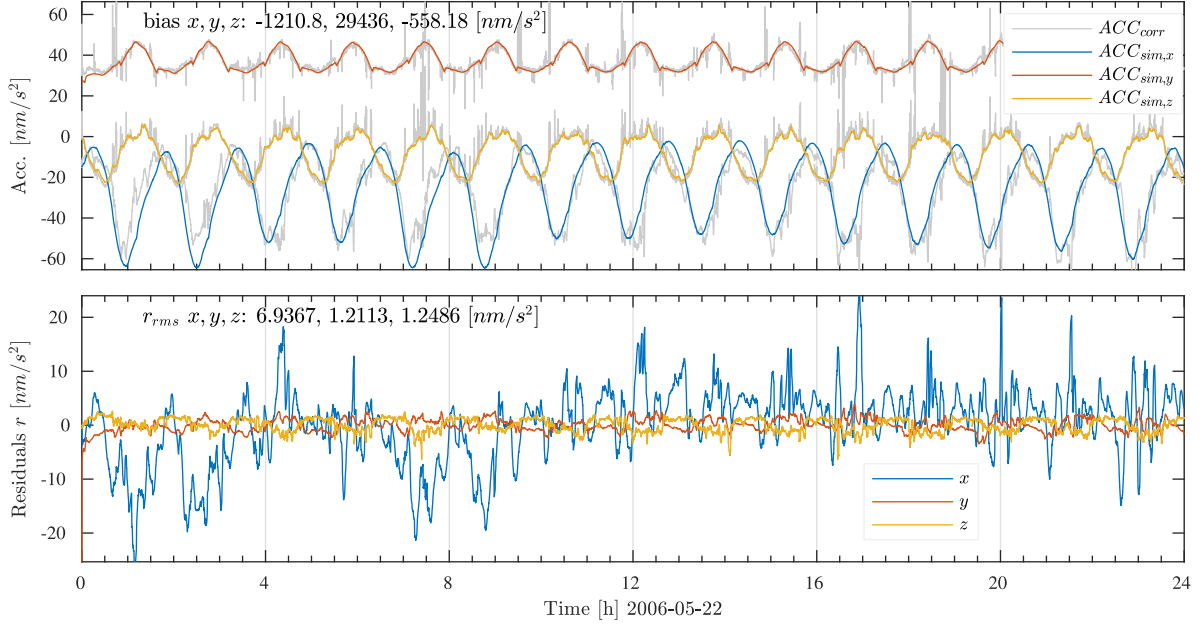


Fig. 2. (Top) Calibrated ACC1B data  $ACC_{corr}$  with modeled non-gravitational accelerations  $ACC_{sim}$  from GRACE A. Bias  $\mathbf{b}$  is estimated for one day with const. scale factors from TN-02, the estimated bias values are given in the plot. Accelerations are in satellite fixed science reference frame (SRF). All spikes in ACC1B data refer to attitude thruster firings. (bottom) Resulting residuals of calibration for each axis. A rms residual  $r_{rms}$  as a single measure for one day is given in the plot for each axis, as well.

condition. Especially for atmospheric drag, the altitude and solar activity has an enormous influence on the atmospheric density and thus on the magnitude of the drag forces. In Fig. 3 the individual modeled non-gravitational forces acting on the GRACE A satellite are shown for each axis in the body frame for high and low solar activity (solar activity cf. Fig. 12 in Section 6.2). For similar illumination conditions the *beta'* angles are chosen to be similar (the sign is changed because switch of GRACE A and B).

Most prominent is the change of the drag force of about one order of magnitude for high and low solar activity. In y-direction, drag is up to the size of SRP for the high activity case, whereas in the low activity case it is not significant in y- and z-direction. For low solar activity, radiative and atmospheric forces are about the same size in total. The radiative forces are not affected by changes in the solar activity. Just differences in ALB and IR are visible due to the local cloud and temperature distribution on Earth. Of course, the direct SRP is the biggest radiative force, being the trigger for all others radiative forces. In peaks ALB can reach up to 50% of SRP in the z-direction. The IR force is a bit smaller, but more constant and not affected by eclipses. TRP is mainly following the SPR curve a bit shifted and more smooth, because SRP being the main heater of the satellite. TRP may reach up to 25% of SRP in some cases.

Non-gravitational forces are computed with the satellite simulation tool XHPS, which is a multi-satellite simulator, with several implemented advanced schemes to achieve high fidelity and fast computation.

Within the XHPS preprocessing module, normalized force and torque coefficient look-up tables are generated for a grid of specified incident perturbation directions for a satellite FE model. When calling the force model with a given incident disturbance direction, e.g. Sun direction, the values are interpolated in the look-up tables. The incident disturbance direction is described in polar coordinates in a satellite fixed frame with polar angle  $\theta$  reaching from 0 to  $\pi$  and azimuth angle  $\phi$  from 0 to  $2\pi$ . The preprocessing allows fast computation of complex satellite and perturbation models, once computed, independent of the level of detail of the satellite FE model. A simple and a detailed GRACE FE model and the illumination conditions for one incident direction are shown in Fig. 4.

#### 4.1. Solar radiation pressure

The origin and effects of SRP are well known and the phenomena are modeled considering specular and diffuse reflections and absorption of photons of illuminated satellite surface elements. The incident disturbance direction in satellite body frame  $\mathbf{e}_{inc}$  is described by a unit vector in the polar coordinates  $\theta$  and  $\phi$  by  $\mathbf{e}_{inc} = [\sin(\theta)\cos(\phi), \sin(\theta)\sin(\phi), \cos(\theta)]^T$ . For SRP the incident direction is pointing towards the Sun,  $\mathbf{e}_{inc} = \mathbf{e}_{Sun}$ . The SRP force on each satellite surface element  $k$  can then be expressed by using the surface optical properties and relevant vector components (e.g. Rievers et al., 2012):

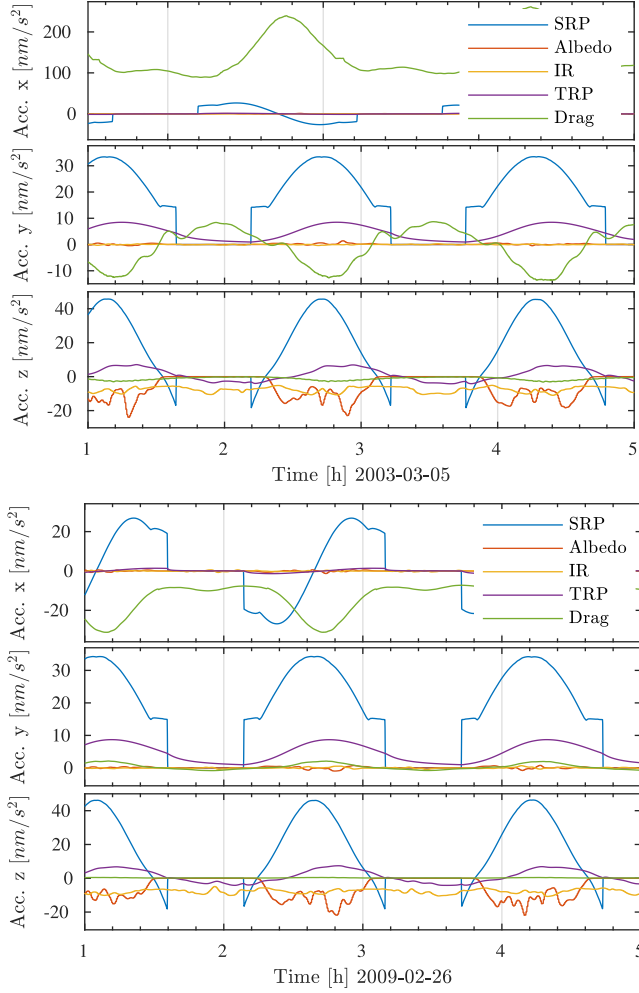


Fig. 3. Individual modeled non-gravitational forces for GRACE A in the body frame for high (top) and low (bottom) solar activity and similar  $\beta'$  angles of  $37.2^\circ$  and  $-35.8^\circ$  (different sign because switch of GRACE A and B).

$$\mathbf{F}_{SRP,k} = -\frac{q_{in}}{c} \cdot f_{shadow,k} A_k \mathbf{e}_{inc} \cdot \mathbf{e}_{N,k} \left[ (\alpha_i + \gamma_{d,k}) \mathbf{e}_{inc} + 2 \left\{ \frac{\gamma_{d,k}}{3} + \gamma_{s,k} \mathbf{e}_{inc} \cdot \mathbf{e}_{N,k} \right\} \mathbf{e}_{N,k} \right], \quad (6)$$

with a surface normal vector  $\mathbf{e}_{N,k}$  expressed in satellite body frame and  $\alpha_k, \gamma_{s,k}, \gamma_{d,k}$  and  $A_k$  being the absorptivity, specu-

lar and diffuse reflectivity coefficients and area of element  $k$ , respectively. The binary factor  $f_{shadow,k}$  indicates if an element is shadowed by another one, which is computed by employing the ray-tracing method.  $c$  is the speed of light. The first factor on the right hand side  $q_{in}$  represents the incoming irradiation at the satellite's position, e.g. the solar flux for SRP. All other terms of the equation depend only on satellite properties. Therefore the equation is evaluated in the preprocessing module for all desired irradiation directions ( $\theta$  and  $\phi$ ) with a chosen step size, without the factor  $q_{in}/c$ . The summed results over all elements  $k$  are then saved as look-up tables. When calling the model for a given incident direction ( $\theta$  and  $\phi$ ),  $q_{in}/c$  is multiplied after interpolation from the look-up tables.  $q_{in}$  is dependent on satellite and Sun position, as well as on the solar constant  $q_{\odot}$ , thus it is not included in the look-up tables. With a given solar constant  $q_{\odot}$  at the distance of one astronomical unit (AU) and Sun's position  $\mathbf{r}_{Sun}$ , an incident power at the satellites position  $\mathbf{r}_{sat}$  can be computed:

$$q_{in} = q_{\odot} \left( \frac{1 \text{ AU}}{\|\mathbf{r}_{sat} - \mathbf{r}_{Sun}\|} \right)^2. \quad (7)$$

In addition, we distinguish the eclipse conditions for given epoch and position of satellite, Earth and Sun.

#### 4.2. Albedo and Earth infrared radiations

Our model is based on CERES SYN1deg Earth observation data. Among others, it provides Earth reflectivity and long wave radiation data for an epoch starting in 2000 up to now. It has a spatial resolution of  $1^\circ$  in longitude and latitude and a time resolution from hourly to monthly. For this study the hourly data is used.

Unlike SRP, where the source of radiation is only one point, for ALB and IR radiation all surface area of the Earth, that is in the field of view (FOV) of a satellite, has to be considered as radiation source. Therefore the Earth is gridded in cells with indices  $ij$ . Radiation from each cell is considered in the model. Based on the Lambertian cosine-law, for ALB and IR a diffuse reflectance of an Earth cell into the hemisphere is assumed (Knocke et al., 1988). Each cell is assigned an area  $A_{ij}$ , a reflectivity  $\rho_{ij}$ , and an outgoing IR flux  $q_{IR,ij}$ .

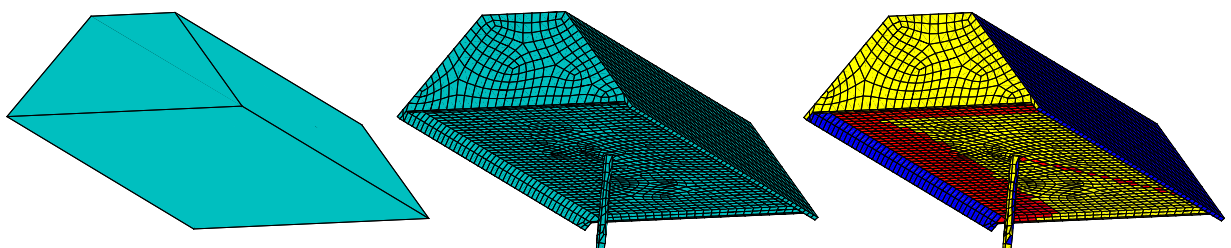


Fig. 4. (Left, middle) Simple six face and detailed FE model. (Right) Illumination conditions of the FE model for one incident direction, yellow: illuminated, blue: not illuminated, red: shadowed. (For interpretation of the references to colour in this figure legend, the reader is referred to the web version of this article.)









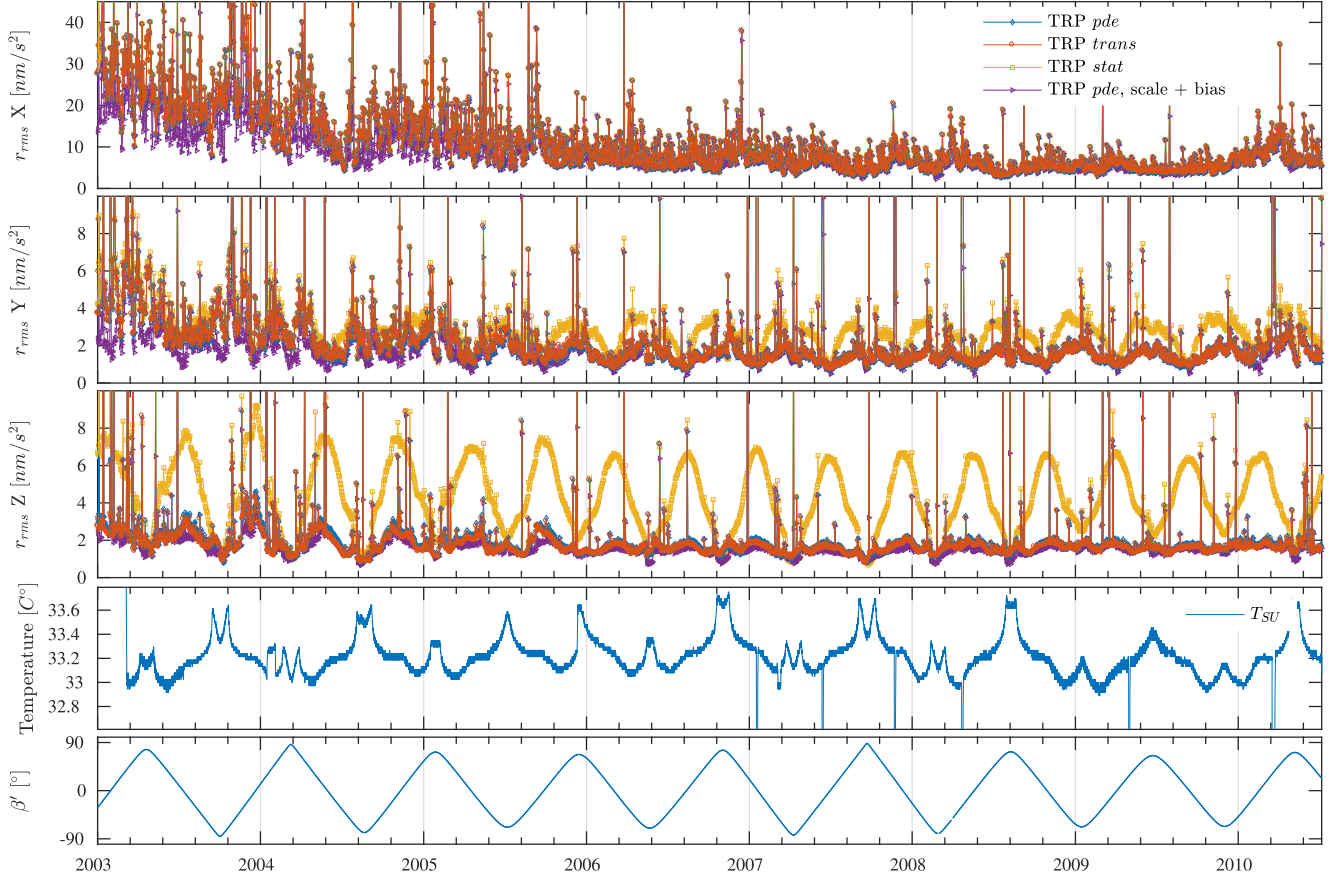


Fig. 10. X-, y- and z-residuals of accelerometer calibration for four different cases: In the first three cases the three different TRP models static (*stat*), transient (*trans*) and *pde* are used in combination with all other non-gravitational force models for bias estimation with constant scale factors  $s_{TIV}$  from Table 1. In the fourth case, additionally the scale factors are also estimated, using the *pde* TRP model. Additionally accelerometer SU temperature from AHK data and the  $\beta'$  angle are shown to point out the correlations. Period 1, GRACE A.

between line of sight and orbital velocity direction of the two satellites, drag also couples in the y- and z-axis, and thus residuals increase also in these directions with higher uncertainty of atmospheric density. For the “quiet” phase from 2006 to 2011 the drag components in y- and z-axis are maximal up to 5% of the whole acceleration, for the last years the drag components in these axes are bigger than the radiative forces. This is causing the increasing residuals also in these axes. For the evaluation of the force models, the first time period is more significant, because drag is less dominant and not superimposing the other effects.

An obvious correlation of the residuals with the  $\beta'$  angle exists, especially for the *stat* TRP model in z- and y-axis. For big  $\beta'$  angles, when there is no eclipse, the results from the static model are very close to these of the more sophisticated transient models (*trans* and *pde*), visible in the small residuals in Figs. 10 and 11 for these periods. This is consistent because the illumination conditions are nearly steady and the satellite surface temperatures are more or less in an equilibrium. With decreasing  $\beta'$  angle, eclipse phases get longer and the illumination conditions for the different surfaces are changing faster. Therefore heating and cooling is getting more significant, what is visible in

a considerable rise of the residuals for the *stat* TRP model, which is not considering these processes. This is resulting in the prominent periodic residuals (cf Fig. 10) with an amplitude of about  $6 \text{ nm}/\text{s}^2$  for z-direction and  $3 \text{ nm}/\text{s}^2$  for y-direction. For the two transient temperature models the resulting residuals are very close, hardly to distinguish in the figure. They also show a slight periodic behavior, but not with such distinct correlation to the  $\beta'$  angle and with a much smaller amplitude of about  $1 \text{ nm}/\text{s}^2$ . In general, the calibration method with the *trans* and *pde* models results in y- and z-residuals between 1 and  $3 \text{ nm}/\text{s}^2$  for the first period (cf. Fig. 10), which is quite remarkable.

The internal power production used as BC for the PDE solution of the *pde* model has a negligible influence on the residuals. Also the bias difference between the 500 W BC and the 250 W BC is small, resulting in a constant bias offset of  $+1 \text{ nm}/\text{s}^2$ . The 250 W BC is used for all further results because the value seems most realistic (Kramer, 2018). The residuals for the *trans* and *pde* models are very similar, but also here the resulting *trans* bias has an offset in z-axis of  $+1 \text{ nm}/\text{s}^2$  to the 250 W *pde* solution. This can be credited to the internal heat production which is mainly radiated from the radiator in radial direction.

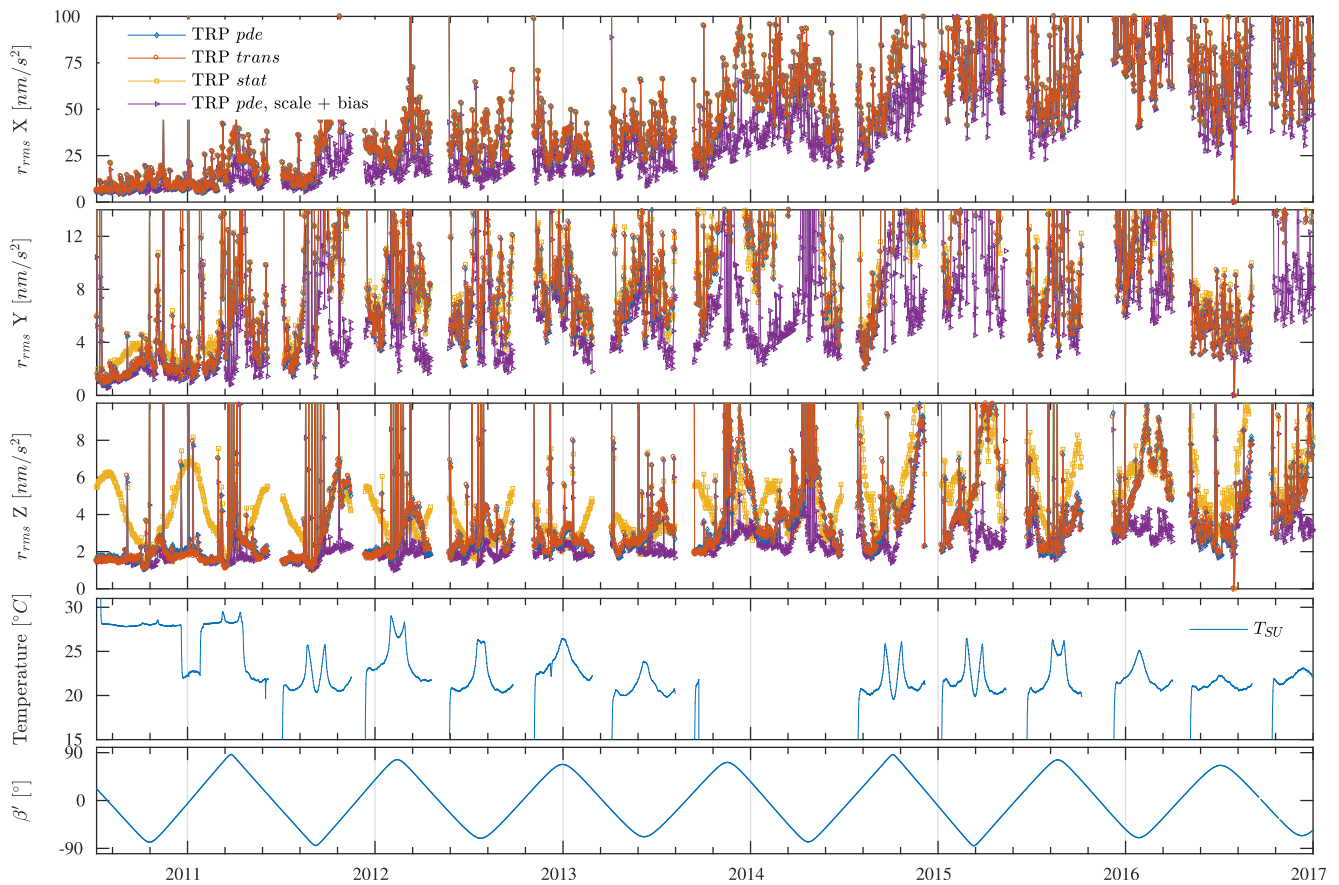


Fig. 11. X-, y- and z-residuals of accelerometer calibration for four different cases: In the first three cases the three different TRP models static (*stat*), transient (*trans*) and *pde* are used in combination with all other non-gravitational force models for bias estimation with constant scale factors  $s_{T\bar{V}}$  from Table 1. In the fourth case, additionally the scale factors are also estimated, using the *pde* TRP model. Additionally accelerometer SU temperature from AHK data and the  $\beta'$  angle are shown to point out the correlations. Period 2, GRACE A.

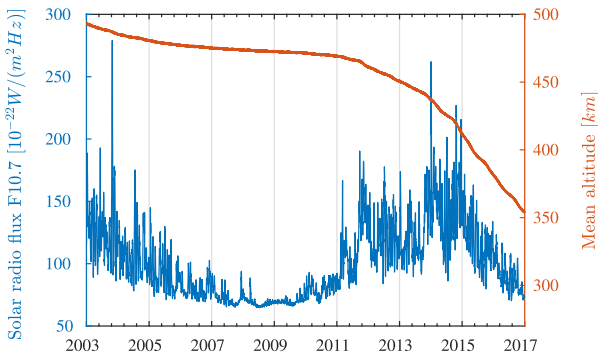


Fig. 12. Solar radio flux (F10.7) and GRACE mean altitude over the whole mission time period.

High gradients in the accelerometer SU temperature ( $T_{SU}$ ) cause a bias drift, happening on time scales smaller than one day, which conflicts with the estimation of constant calibration parameters over one day, and thus resulting in high residuals for these times. These spikes or outliers are obviously visible in the residuals in Figs. 10 and 11. For nearly all outliers in the residuals also the accelerometer SU temperature shows a spike or a high gradient. The different accelerometer axes are not necessarily

coupling to the same temperature spikes. A further reason for outliers are maneuvers of the satellite, happening more often in the second time period. Also the number of outliers has increased after the temperature control shutdown (in 2011), which changed the range of SU temperature variation with one order of magnitude (cf. Figs. 10 and 11). In the second period outliers are also produced by the shutdown of science instruments (for small  $\beta'$  angles). After activating the accelerometer again, the SU temperature needs about three to five days until it stabilizes and the assumption of constant bias over one day is sustainable again.

We decided to use the constant estimation for one day to be able to compare and validate our models with the accelerometer data, which is not reasonable when fitting too many parameters. For GRACE accelerometer calibration, it would be advantageous to fit a linear or a quadratic bias function over one day in times with high accelerometer SU temperature gradients.

The estimation of the additional scale calibration parameter does not significantly decrease the residuals. Mainly an effect on the x-direction is visible, where it partly adapts for density and drag uncertainties. But in general

the scale factors attain unrealistic high and low values. Especially if the absolute accelerations are rather small, e.g. for small  $\beta'$  angles in y-direction, and if the shape of the curves between measured and modeled non-gravitational forces shows bigger differences, e.g. for several periods in x-direction and the later mission. The x-scale factor is shown in Fig. 13. The estimation of bias and scale together is difficult. Bias and scale are hard to delineate, up to a certain amount, the data may be similarly well adjusted by a change of scale or bias. From our analysis we have to conclude, that the method is not sensitive enough to estimate reasonable scale factors. Hence we decided to use the constant scale factors for the calibration as also done in various studies, e.g. Calabia et al. (2015), Bezděk (2010) and Van Helleputte et al. (2009).

### 6.3. Comparison of calibration parameters

Calibration results from three other studies with different approaches are generously provided for comparison: 1. a GPS based calibration (Calabia et al., 2015), tagged *Calabia*, 2. co-estimated calibration parameters within the GFR process (Mayer-Gürr et al., 2016), tagged *Graz gfr*, and 3. another force model based method (Klinger and Mayer-Gürr, 2016), tagged *Graz sim*. Additionally the calibration from TN-02 is used for comparison (*TN-02*). It is just shown for the valid period until 2009, and used with corrected calibration equation (cf. Section 2.1). As a basis for the comparisons, the results from this study with *pde* TRP model and constant scale factors  $s_{TN}$  are used (*XHPS*).

In order to compare the results, some processing is needed to be done. Bias values from *Calabia* are estimated with a scale factor of 1 in Eq. (1), also estimated for one day, like in this study. Thus estimated bias values have a simple offset of  $ACC1B(1 - s_{TN})$  to *XHPS*, that needs to be considered. For *Graz gfr* and *Graz sim*, calibrated accelerations are obtained with a scale matrix as well as a time dependent bias, estimated with cubic splines for each six hours epochs (Mayer-Gürr et al., 2016; Klinger and Mayer-Gürr, 2016). To compare these results, a constant offset for one day between both calibrated accelerometer data ( $ACC_{corr}$ ) is determined in terms of least squares. For *Graz gfr* the mean residuals for this estimation (over the whole time period) are 2.1, 12.5 and 9.3 nm/s<sup>2</sup> for x-,

y- and z-axis, respectively. Meaning a rather large variation of accelerometer bias over a day in y- and z-direction within the GFR process using the time variable bias estimation. For the x-direction the bias variation is much smaller.

The same least squares method is used to compare the results for the other model based study *Graz sim*. Here the mean residuals are 8.6, 4.8 and 0.56 nm/s<sup>2</sup> for x-, y- and z-axis, being the other way around as for GFR processing, with the biggest differences in x-axis. This may likely be explained by the fact that the variable bias is compensating for atmospheric density model uncertainty.

The bias difference with respect to the results from this study (*XHPS*) are shown in Figs. 14 and 15 for GRACE A, for x-, y-, and z-axes, again for the two prescribed time periods. Y-axis is shown twice with different scale because of the big differences of (*TN-02*) in that direction.

The results for the x-axis from *Calabia* and *Graz gfr* are very close, also *TN-02* results follow mainly the same trend. This may be reasoned because all originate from a POD process. The other model based study *Graz sim* shows similar trend and magnitude in x-direction as for this study. The distinct offset between POD based methods and *XHPS* from 2003 to 2006 and the much smaller offset from 2006 to 2011 in the other direction is discussed more detailed in Section 6.4.

In the analysis from *Calabia* the daily bias is estimated in steps for 15 days, but for the year 2006 where it is done for each day. In between the 15 days, the bias is linear interpolated. This causes some bigger differences especially in y-direction, where the absolute change of bias with respect to time is the biggest, and thus the 15 day interpolation is not as accurate. For the year 2006, where bias is estimated for each day, the differences in this axis are much smaller than for the rest (cf. Fig. 14).

The same is true for *TN-02* calibration. The quadratic fit for about 8 years can not depict small changes, nor changes on  $\beta'$  angle period scale. Therefore, especially for y-axis, with the biggest absolute bias changes, the differences are quite big. A distinct correlation between the *TN-02* y-bias difference and the accelerometer SU temperature (cf.  $T_{SU}$  in Fig. 10) is visible.

For *Graz sim* and *Graz gfr*, a correlation with the  $\beta'$  angle in y-axis is obvious. Completely excluding TRP forces in this study for the estimation produces a similar sinusoidal bias difference with an amplitude of about 8 nm/s<sup>2</sup>. Because TRP forces are not considered in *Graz sim*, this is likely the source of this oscillating difference. The *Graz sim* calibration is used as a priori estimate in the GFR process, therefore *Graz gfr* may deliver similar periodic oscillations. At the end of the year 2005, as well as in mid 2014, the flip maneuver of GRACE A and B is visible, causing the sign switch of this oscillation in *Graz sim* as well as in *Graz gfr*.

The offset in z-direction between the force model based studies (*XHPS* and *Graz sim*) and *Calabia* and *Graz gfr* is

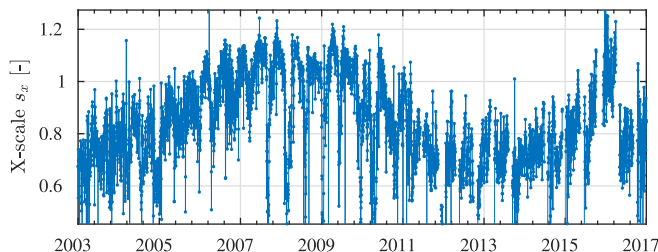


Fig. 13. Estimated x-scale factor when estimating scale and bias calibration parameters, GRACE A.

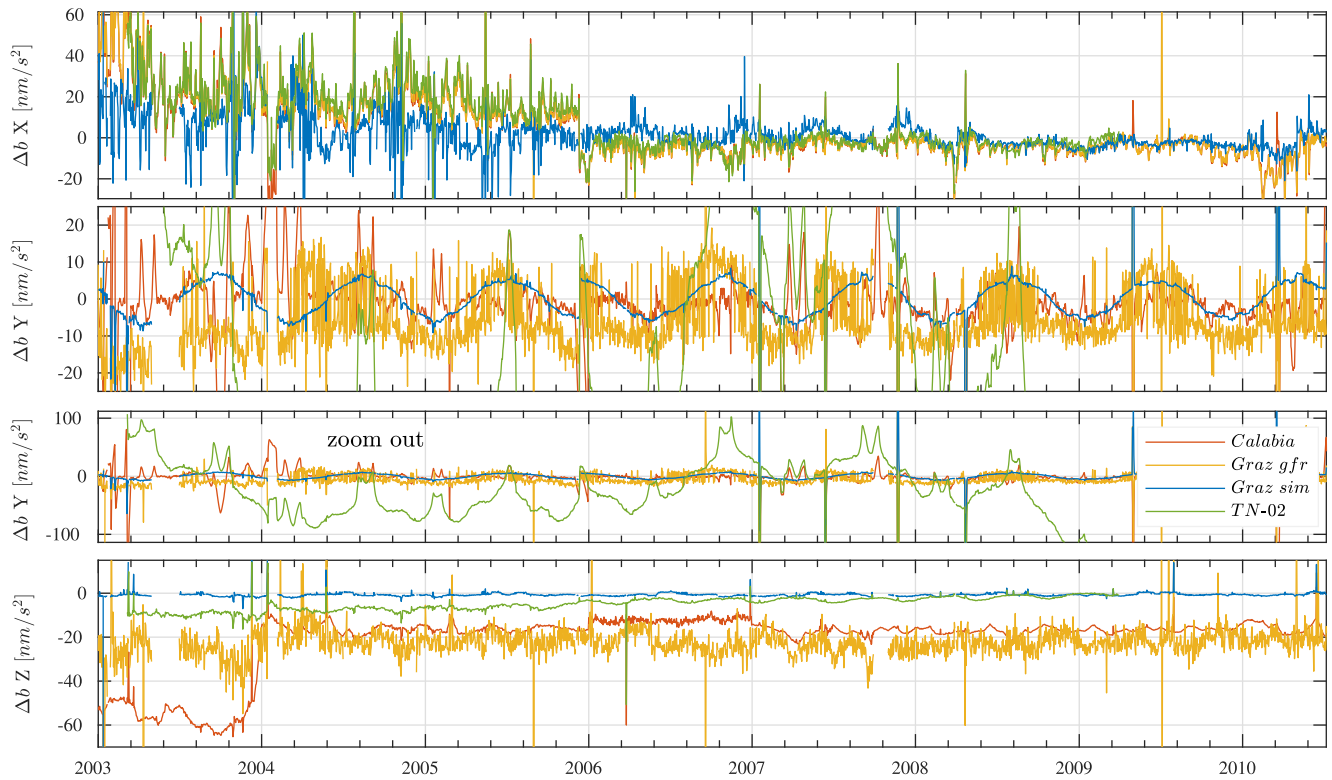


Fig. 14. Comparison of the daily bias results from the different calibration methods. Shown are the bias differences with respect to results from this study (*XHPS*) for GPS based calibration (Calabia et al., 2015) (Calabia), GFR based calibration (Mayer-Gürr et al., 2016) (Graz *gfr*), a different method based on modeled accelerations (Klinger and Mayer-Gürr, 2016) (Graz *sim*) and for calibration from TN-02 (Bettadpur, 2009) (TN-02) for x-, y- and z-axis. Y-axis is shown twice with different axis scale to better see the details. TN-02 results are shown for the valid period until April 2009. Note the different calibration equation in the GRACE TN-02, cf. Section 2.1. Period 1, GRACE A.

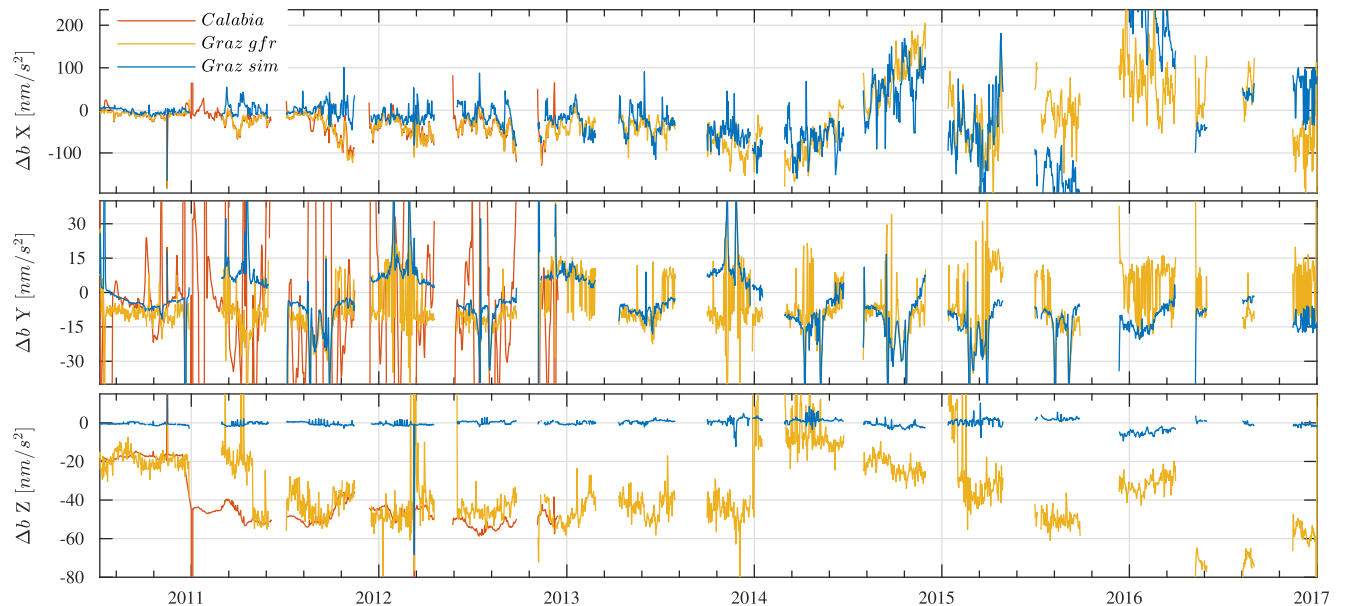


Fig. 15. Comparison of the daily bias results from the different calibration methods. Shown are the bias differences with respect to results from this study (*XHPS*) for GPS based calibration (Calabia et al., 2015) (Calabia), GFR based calibration (Mayer-Gürr et al., 2016) (Graz *gfr*), and a different method based on modeled accelerations (Klinger and Mayer-Gürr, 2016) (Graz *sim*) for x-, y- and z-axis. Period 2, GRACE A.







- Peterseim, N., Flury, J., Schlicht, A., 2012. Magnetic torquer induced disturbing signals within GRACE accelerometer data. *Adv. Space Res.* 49, 1388–1394. <https://doi.org/10.1016/j.asr.2012.02.013>.
- Rievers, B., Lämmerzahl, C., 2011. High precision thermal modeling of complex systems with application to the flyby and Pioneer anomaly. *Ann. Phys.* 523.
- Rievers, B., Kato, T., van der Ha, J., Lämmerzahl, C., 2012. Numerical prediction of satellite surface forces with application to Rosetta. In: AAS/AIAA Spaceflight Mechanics Meeting, number AAS 12-180.
- Rievers, B., List, M., Bremer, S., 2016. Advanced thermal radiation pressure modeling and its benefits for the MICROSCOPE mission. *Adv. Astr. Sci.* 158, 2997–3012.
- Tapley, B.D., Bettadpur, S., Watkins, M., Reigber, C., 2004. The gravity recovery and climate experiment: Mission overview and early results. *Geophys. Res. Lett.* 31, L09607. <https://doi.org/10.1029/2004GL019920>.
- Touboul, P., Willemont, E., Foulon, B., Josselin, V., 1999. Accelerometers for CHAMP, GRACE and GOCE space missions: Synergy and evolution. *Bollettino di Geofisica ed applicata* 40 (3-4), 321–327.
- Touboul, P., Foulon, B., Rodrigues, M., Marque, J.P., 2004. In orbit nano-g measurements, lessons for future space missions. *Aerosp. Sci. Technol.* 8, 431–441. <https://doi.org/10.1016/j.ast.2004.01.006>.
- Van Helleputte, T., Visser, P., 2008. GPS based orbit determination using accelerometer data. *Aerosp. Sci. Technol.* 12, 478–484. <https://doi.org/10.1016/j.ast.2007.11.002>.
- Van Helleputte, T., Doornbos, E., Visser, P., 2009. CHAMP and GRACE accelerometer calibration by GPS-based orbit determination. *Adv. Space Res.* 43, 1890–1896.
- Wielicki, B.A., Barkstrom, B.R., Harrison, E.F., Lee III, R.B., Smith, G. L., Cooper, J.E., 1996. Clouds and the Earth's Radiant Energy System (CERES): An Earth observing system experiment. *Bull. Amer. Meteor. Soc.* 77, 853–868.
- Wöske, F., Kato, T., List, M., Rievers, B., 2016. Development of a high precision simulation tool for gravity recovery missions like GRACE. *Adv. Astr. Sci.* 158, 2445–2457.
- Wu, S.C., Yunck, T.P., Thornton, C.L., 1991. Reduced-dynamic technique for precise orbit determination of low earth satellites. *J. Guidance, Control, Dynam.* 14 (1), 24–30.